Heliyon

Molecular autopsy: using the discovery of a novel de novo pathogenic variant in the KCNH2 gene to inform healthcare of surviving family

Jingyun Dong [c,d,e], Nori Williams [a], Marina Cerrone [f], Christopher Borck [b], Dawei Wang [a], Bo Zhou [a], Lucy S. Eng [a], Ekaterina Subbotina [c,d,e], Sung Yon Um [a], Ying Lin [a], Kevin Ruiter [a], Lisa Rojas [a], William A. Coetzee [c,d,e], Barbara A. Sampson [b], Yingying Tang [a],*

[a] *Molecular Genetics Laboratory, New York City Office of Chief Medical Examiner, USA*

[b] *Department of Pathology, New York City Office of Chief Medical Examiner, USA*

[c] *Department of Pediatrics, NYU School of Medicine, USA*

[d] *Department of Biochemistry and Molecular Pharmacology, NYU School of Medicine, USA*

[e] *Department of Physiology and Neurosciences, NYU School of Medicine, USA*

[f] *Cardiovascular Genetics Program, Leon H Charney Division of Cardiology, NYU School of Medicine, NY, USA*

* Corresponding author.
E-mail address: ytang@ocme.nyc.gov (Y. Tang).

Abstract

Background: Molecular testing of the deceased (Molecular Autopsy) is an overlooked area in the United States healthcare system and is not covered by medical insurance, leading to ineffective care for surviving families of thousands of sudden unexpected natural deaths each year. We demonstrated the precision management of surviving family members through the discovery of a novel *de novo* pathogenic variant in a decedent.

Methods: Forensic investigation and molecular autopsy were performed on an 18-year-old female who died suddenly and unexpectedly. Co-segregation family study

of the first-degree relatives and functional characterization of the variant were conducted.

Findings: We identified a novel nonsense variant, NP_000229.1:p.Gln1068Ter, in the long QT syndrome type II gene *KCNH2* in the decedent. This finding correlated with her ante-mortem electrocardiograms. Patch clamp functional studies using transfected COS-7 cells show that hERG-ΔQ1068 has a mixed phenotype, with both gain- (negative voltage shift of steady-state activation curve, the positive shift of the steady-state inactivation curve, and accelerated activation) and loss-of function (reduced current density, reduced surface expression and accelerated deactivation) hallmarks. Loss of cumulative activation during rapid pacing demonstrates that the loss-of-function phenotype predominates. The wild-type channel did not rescue the hERG-ΔQ1068 defects, demonstrating haploinsufficiency of the heterozygous state. Targeted variant testing in the family showed that the variant in *KCNH2* arose de novo, which eliminated the need for exhaustive genome testing and annual cardiac follow-up for the parents and four siblings.

Interpretation: Molecular testing enables accurate determination of natural causes of death and precision care of the surviving family members in a time and cost-saving manner. We advocate for molecular autopsy being included under the healthcare coverage in US.

Keywords: Clinical genetics, Genetics, Cell biology, Evidence-based medicine, Pathology, Molecular biology

1. Introduction

Medical genetics and genomic testing is emerging onto the center stage in human health, including carrier screening, preimplantation genetic diagnosis, non-invasive prenatal screening, newborn screening, and diagnosis of common or rare heritable conditions. However, the current healthcare system in the United States lacks proper policy and procedures to support some essential medical genetics services. One of the overlooked areas is postmortem genetic testing of decedents who died naturally, suddenly, and unexpectedly at young ages (molecular autopsy). The value of molecular autopsy in the determination of underlying natural causes of death, and the subsequently improved healthcare of surviving family members has been shown in numerous case reports [1, 2, 3]and cohort studies [4, 5, 6]. However, primarily due to lack of coverage from medical insurance, genetic testing of the deceased is not routinely performed in most of the United States, as it is in our Office in the City of New York, leaving thousands of cases unsolved each year and at-risk family members on the hook. This leads to costly and ineffective management of surviving families.

In this study, we present the discovery of a novel *de novo* pathogenic variant in *KCNH2*, a long QT syndrome gene, in a young decedent who died suddenly and

unexpectedly. We demonstrate how molecular autopsy enables effective precision healthcare to surviving family members which can only be achieved through molecular testing of affected decedents.

With the recently published statement of "Considerations in healthcare reform for patients and families with genetic diseases" by the Board of Directors of the American College of Medical Genetics and Genomics [7], we advocate that molecular autopsy should be included under healthcare coverage in the United States as it directly impacts surviving family members.

2. Materials and methods

2.1. Case presentation and forensic investigation

An 18-year-old Asian female was found dead in her bedroom in New York City by her family. 911 was called and EMS pronounced the death without medical intervention due to rigor mortis.

Bodies of deceased persons are brought to the New York City Office of Chief Medical Examiner (NYC-OCME) because the law requires that the Chief Medical Examiner investigate deaths of persons dying from criminal violence, by accident, by suicide, suddenly when in apparent health, when unattended by a physician, in a correctional facility, or in any suspicious or unusual manner. The medical examiner is responsible for determining the cause and manner of death. OCME forensic investigation of sudden death includes: scene investigation and family interview (by certified physician assistants), complete gross autopsy, detailed cardiac pathology and neuropathology examinations and microscopic evaluation of important organs, toxicological tests, microbiological tests (in infants), metabolic screening tests (in infants), and medical record review. After these investigations, if the underlying cause of death remains unclear, or if there is suspicion of channelopathy or cardiomyopathy, molecular analysis of a panel of 95 cardiac arrhythmogenic genes by next-generation sequencing (NGS) will be performed [5].

2.2. Postmortem molecular testing

NYC-OCME's in-house College of American Pathologists (CAP)-accredited Molecular Genetics Laboratory performed the testing. NGS testing and Sanger sequencing methods were reported previously [5, 8]. Nomenclature of Sequence variants follows the Human Genome Variant Society (HGVS) recommendations [9]. Variant interpretation follows the American College of Medical Genetics and Genomics and the Association for Molecular Pathology (ACMG-AMP) guidelines published in 2015 [10]. Genetic results include variant location on human-genome reference (GRCh37/hg19). The Institutional Review Board of the New York City Department of Health and Mental Hygiene approved this study.

2.3. Genetic counseling and family study

After postmortem molecular testing was completed, OCME's in-house board-certified genetic counselor provided counseling to the parents and four full-siblings of the decedent, and referred them to the Cardiovascular Genetics Program Inherited Arrhythmias Clinic at NYU School of Medicine for clinical evaluation and targeted variant testing. Informed Consent was obtained from all living family members. Genetic testing of family members was performed through a New York State approved commercial company (Invitae Inc.).

2.4. Site-directed mutagenesis

The full-length wild-type human ERG cDNA (hERG or Kv11.1; NP_000229.1; clone #1160) in the pRcCMV vector was a gift from Dr. Minoru Horie (Shiga Medical Center, Shiga, Japan). Site-directed mutagenesis, to generate hERG-ΔQ1068, was performed by Genscript (Piscataway, NJ, USA).

2.5. Cell culture

COS-7 or HEK-293 cells were grown in Eagle's Modified Essential Medium (EMEM) (Thermo Fisher Scientific, Waltham, MA), supplemented with heat-inactivated 10% Fetal Bovine Serum (FBS) and penicillin (100 IU/mL) and streptomycin (100 μg/mL). Cells were grown in 35 mm culture plates and, unless stated otherwise, transfected at 70−80% confluence using Lipofectamine 2000 reagent (Life Technologies, Carlsbad, CA) with wild-type hERG, hERG-ΔQ1068, or wild-type hERG plus hERG- ΔQ1068 cDNAs. In each reaction, 0.1 μg of a GFP plasmid was included to allow visualization of successfully transfected cells by fluorescence microscopy. Patch clamping was performed 48 hours after transfection.

2.6. Whole-cell patch-clamp recordings

Membrane current were recorded in the whole-cell configuration at room temperature with Axopatch 200B (Molecular Devices, San Jose, CA), low-pass filtered with 8-pole Bessel filter (-3 dB @ 1 Hz), digitized (3 kHz; DigiData 1550 A, Axon Instruments) and recorded using pClamp v10.5 software (Molecular Devices). Patch electrodes were manufactured using borosilicate glass (1.5 mm OD; World Precision Instruments, Sarasota, FL) and had tip resistances of 2−4 MΩ when filled with (in mmol/L): 110 KCl, 1 $MgCl_2$, 1 EGTA, 10 HEPES, 2 MgATP and pH 7.2, adjusted with KOH. The bath solution consisted of (in mmol/L): 137 NaCl, 5.4 KCl, 1.8 $CaCl_2$, 0.5 $MgCl_2$, and 10 HEPES, with pH 7.4 adjusted with NaOH. Data were not corrected for the liquid junction potential. The whole-cell capacitance and series resistance were compensated to levels greater than 80%. Currents were corrected for cell size by dividing by the cell capacitance and expressing as pA/pF.

2.7. Western blotting

Transiently transfected were harvested using RIPA buffer (Sigma-Aldrich, St. Louis, MO) supplemented with HaltTM protease inhibitor cocktail (Thermo Fisher Scientific, Waltham, MA). Cells were homogenized on ice (3 bouts of 15 pulses at 50 % strength) using a Microson XL sonicator (Qsonic, Newtown, CT) and centrifuged for 15 min (14,000 x g at 4 °C). The protein concentration of the supernatant was measured with a BCA Protein Assay Kit (ThermoFisher Scientific), aliquoted and stored at -80 °C. Before use, 20 μg protein was mixed with sample buffer (Thermo Fisher Scientific) containing 5 % β-mercaptoethanol and 3% sodium dodecyl sulfate (SDS) and kept at room temperature prior to resolving with a 4−20 % polyacrylamide gradient gel. The fractionated proteins were transferred to polyvinylidene difluoride (PVDF) membranes (Bio-Rad, Hercules, CA) using a semi-dry system Trans-Blot Turbo (Bio-Rad). Blocking was performed with 5% fat free milk in TBS-Tween (0.01%) for 1 h, followed by incubation with rabbit polyclonal anti-potassium channel Kv11.1 extracellular antibody (P0749, 1:2000, Sigma-Aldrich) overnight at 4 °C and goat anti-rabbit lgG-HRP secondary antibody (sc-2004, 1:20,000, Santa Cruz Biotechnology), dissolved in blocking buffer, for 1 h at room temperature. Detection was performed with chemiluminesence using Super-Signal West Dura (Thermo Fisher Scientific) and documentation with a CCD camera system (Kodak SRX-101A). Analysis of band intensities was performed using ImageJ2 software [11].

2.8. Surface biotinylation assay

Transfected cells were washed twice with ice-cold Hank's balanced salt solution and biotinylated for 30 min using PBS containing 0.25 mg/mL of EZ Link Sulfo-NHS-SS-Biotin (Pierce Thermo Fisher Scientific). Excess biotin was removed by washing twice with PBS and quenched by 5 min incubation with 100 mM glycine in PBS. Cells were scraped from the dish and washed twice with TBS by centrifugation (5 min at 1000 x g). The pelleted cells were lysed with 100 μl RIPA buffer (Sigma-Aldrich, St. Louis, MO) supplemented with HALT Protease Inhibitor Cocktail (Thermo Fisher Scientific). All steps were performed at 4 °C. The biotinylated proteins were mixed with 2x Laemmli sample buffer (Bio-Rad, Hercules, CA) with 5% β-mercaptoethanol at room temperature for 1 h and analyzed by Western blotting.

2.9. Data analysis

Patch clamp data were analyzed using pClamp 10.5 software and plotted using SigmaPlot software (Systat Software Inc, San Jose, CA). All averaged data are expressed as mean ± SEM. Statistical comparisons were performed using Student's t-tests, and statistical significance was assumed when $p < 0.05$.
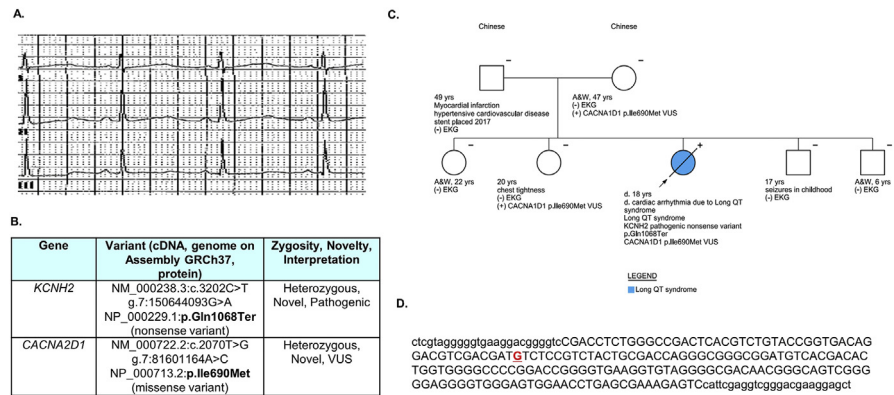
3. Results

3.1. Cause of death determination through forensic examinations

The results of comprehensive forensic studies are summarized in Table 1. Scene investigation found no indications of trauma, foul play or other suspicious or untoward circumstances. Gross and microscopic autopsy results, as well as toxicology tests are essentially negative.

Medical records review showed that the decedent was seen by a cardiologist for asymptomatic prolonged QT. On her initial EKG the decedent's QT/QTc was 436/518 ms with normal sinus rhythm at 85 bpm (Fig. 1A), and her prolonged QT was confirmed by subsequent exercise stress test, where she showed generalized fatigue at peak, but no other symptoms. Her QT-interval was prolonged at baseline and in the recovery phase with a QT of 370 msec and a QTc of 638 msec in the 4th

Table 1. Results of forensic examinations.

Studies	Sources	Results	Conclusion
Scene	NYPD detective	No obvious indications of trauma, foul play or other suspicious/untoward circumstances.	Natural Death
	Death Scene Investigations	No evidence of drug or ETOH abuse in bedroom. No notes, weapons, or other indications of suicidality or foul play. A few medications found including doxycycline. No cardiac medications found. On a desk were documents from a cardiology appointment. Reason for visit was asymptomatic prolonged QT. Documents indicate that the decedent was NOT started on any Beta Blockers or other medications and was just given a list of medications to avoid, pending outcome of stress testing.	
	Body	No evidence of acute trauma on exam.	
	Family interview	Decedent had no psychiatric or substance abuse issues and was a generally happy, healthy, busy college student.	
Autopsy	Gross Examination	Negative	Negative
	Microscopy	Only hepatic steatosis. Heart is normal.	
Toxicology	Femoral blood	none detected for the screened drugs, including ethanol, benzoylecgonine, barbiturates, oxycodone, opiates, amphetamines, benzodiazepines, methadone, cannabinoids, fentanyl, and a group of basic drugs	Negative
	Vitreous Humor	Normal range	
History	Medical records	Abnormal EKG with prolonged QT interval Exercise stress test with prolonged QT interval	Prolonged QT on EKG
Molecular Testing	Non-formalin fixed post-mortem cardiac tissue	Novel nonsense variant in *KCNH2* gene (Long QT syndrome), Heterozygous, likely pathogenic	Likely Pathogenic Variant in LQT gene *KCNH2*

Fig. 1. Key Findings to Establish Cause of Death in the Decedent and Results of Family Study (A). Ante-mortem EKG showed normal sinus rhythm with a heart rate of 85 bpm and prolonged QT interval QTc = 518 ms. (B) molecular testing results of the index; (C) family study results. Index is shown as blue circle. (+) or (-) above the pedigree symbols denotes presence or absence of the pathogenic variant in *KCNH2*; Status of EKG and targeted variant testing results of the *CACNA2D1* VUS is shown below the symbols (D) DNA sequences surrounding the de novo variant in *KCNH2* (underscore in red).

minute of recovery. There is high likelihood of having long QT syndrome type 1 or type 2 in patients with a QTc ≥480 msec at minute 4 of recovery [12] as noted by the cardiologist. She did not come to the scheduled follow-up appointment and passed away without any medical intervention.

Molecular analysis of 95 cardiac arrhythmogenic genes revealed a novel nonsense variant NP_000229.1:p.Gln1068Ter in *KCNH2*, a ClinGen-curated Long QT syndrome Type 2 gene (Fig. 1B). This variant is classified as a pathogenic variant (see the section "Variant Classification using 2015 ACMG-AMP guidelines" below). In addition, a novel variant of uncertain significant (VUS) was found in *CACNA2D1* (an auxiliary subunit of the cardiac L-type Ca^{2+} channel), a gene pending ClinGen's curation.

Collectively, the results from comprehensive forensic studies, medical records review and molecular testing support that the cause of death of the 18-year-old decedent was cardiac arrhythmia due to long QT syndrome caused by the pathogenic variant in the *KCNH2* gene.

3.2. Family study revealed the novel nonsense variant in *KCNH2* arose de novo

Baseline EKG of the parents and the four siblings were normal and none exhibited prolonged QT (Fig. 1C). Targeted testing for the two variants found in the decedent showed that neither parents nor the four siblings in the family harbored the pathogenic variant p.Gln1068Ter in *KCNH2*; therefore, the variant most likely arose *de novo* (nonpaternity is denied, but paternity test was not performed). The novel VUS in *CACNA2D1* was identified in the mother and one of the siblings who are both asymptomatic with negative EKG.

Upon examining 200 bp sequences surrounding the variant site (Fig. 1D), no CpG islands were found (http://www.bioinformatics.org/sms2/cpg_islands.html) and the variant G to A change is not part of the CpG dinucleotides.

3.3. *In vitro* functional characterization of the novel de novo nonsense variant in *KCNH2*

To understand the mechanism of pathogenicity, we performed functional studies for the novel *de novo KCNH2* variant. The gene product of *KCNH2* is a K^+ channel α-subunit named human ERG (hERG), which we shall use here.

3.3.1. hERG-*ΔQ1068* decreases the current density and negatively shifts the activation voltage threshold

We have introduced a nucleotide change in full-length human ERG (hERG) cDNA with site-directed mutagenesis to generate the hERG-ΔQ1068 cDNA construct. Wild-type (WT) hERG or hERG-ΔQ1068 were expressed in COS-7 cells and whole-cell currents were recorded using standard patch clamp methods. No significant currents were recorded in untransfected COS-7 cells (data not shown). In contrast, transfected COS-7 cells exhibited prototypical outward currents during depolarizing pulses. The currents measured at the end of the depolarizing test pulses, corrected for cell capacitance, were plotted as a function of the test potential and exhibited functional outward rectification, which is a typical feature of hERG currents (Fig. 2). The current density of hERG-ΔQ1068 was significantly smaller compared to wild-type for voltages beyond 0 mV. During the repolarization step to -50 mV, large decaying deactivation tail currents were observed (Fig. 2A, B). The voltage-dependence of tail current densities was sigmoidal, and significantly smaller for hERG-ΔQ1068 when compared to wild-type (Fig. 2C). Steady-state activation curves were constructed by normalizing the tail currents to the largest measured tail current (Fig. 2D), which revealed that the hERG-ΔQ1068 activated at more negative voltages compared to wild-type. The voltage for half-maximal activation was 4.1 ± 1.07 mV (n = 7) and -10.5 ± 0.44 mV (n = 7; $p < 0.05$) respectively for wild-type and hERG-ΔQ1068. To determine whether ΔQ1068 affects the hERG channel independent of activation gating properties, we measured the full-activated current-voltage relationship (Fig. 2E and F). Channels were fully opened by clamping to +60 mV, followed by repolarization to various test voltages. The peak amplitude of the tail current, plotted as a function of the test voltage, exhibited inward rectification and showed that the reversal potential of hERG-ΔQ1068 was similar to wild-type. The fully-activated current was decreased at both positive and negative voltages, suggesting that the number of surface channels is decreased by ΔQ1068.
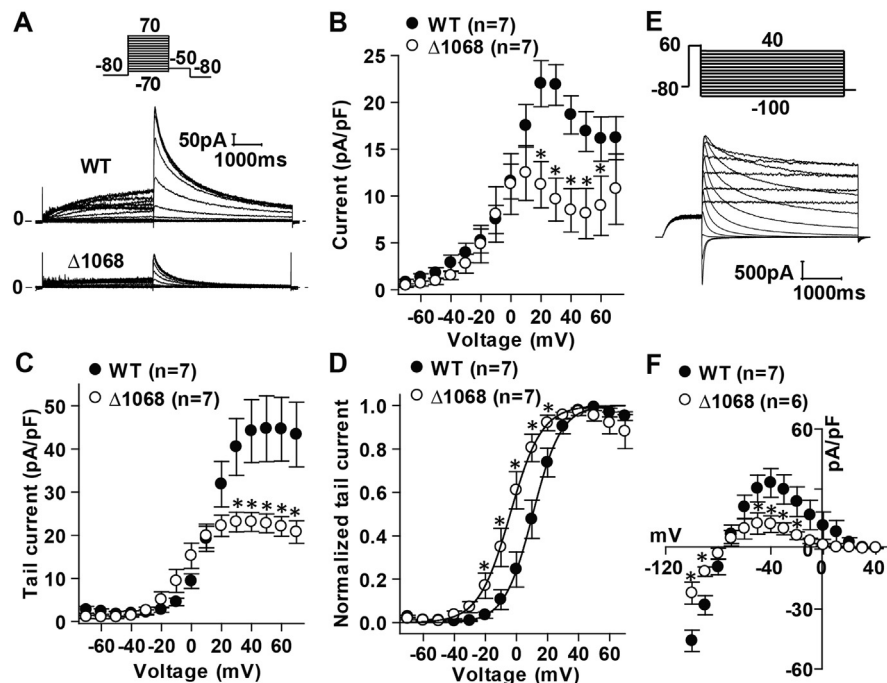
Fig. 2. Activation Properties and Fully-activated Current-voltage Relationships. COS-7 cells were transfected with wild-type hERG or hERG-ΔQ1068 cDNAs and subjected to whole-cell patch clamping. (A) Channels were activated by 4 s conditioning steps, applied at 0.05 Hz, to voltages between -70 mV to +70 mV. Tail currents were recorded during a 5 s test pulse at -50 mV. (B) Currents at the end of the conditioning pulses were plotted as a function of the conditioning voltage. (C) Tail current amplitude density recorded during the test pulse to -50 mV. (D) Normalized tail currents, plotted as a function of the conditioning voltage. Data points were subjected to curve fitting to a Boltzmann equation, $1/[1 + exp[(V_m - V_{1/2})/k]]$, where V_m is the membrane potential, $V_{1/2}$ is the voltage of half-maximal activation, and k represents a slope factor. (E) Representative recording of the fully-activated hERG currents. Membrane currents were elicited by a 1 s depolarizing pulse to +60 mV repeated at 0.05 Hz, followed by variable 4 s test pulses between -100 mV and +40 mV, with 10 mV increments, to a final step to -80 mV. (F) Maximal tail current amplitudes during the variable test pulses were plotted as a function of the test pulse potential. Data points represent mean ± SEM. *$p < 0.05$ with Student's t-test.

3.3.2. Reduced surface expression of hERG-ΔQ1068 channels

We used biochemical approaches to directly measure hERG surface expression. In an initial experiment, HEK-293 cells were transfected with 0.5 µg of WT or ΔQ1068 hERG cDNAs. Western blotting of cell lysates revealed an endogenous 135 kDa band in untransfected cells, with the appearance of a 150 kDa band in WT transfected cells. The 150 kDa band represents a mature form of the protein since it was Endo-H resistant, but sensitive to PNGase F (Fig. 3A). As expected, the Endo-H resistant band of ΔQ1068 hERG was slightly smaller in size (due to the C-terminal truncation) and appeared a less intense than WT, suggestive of a trafficking defect. Curiously, hERG-ΔQ1068 also migrated at a molecular size of ∼120 kDa, which is specific since it is not present in untransfected cells. The identity of this 120 kDa band is unknown and it may be a proteolytic cleavage fragment. To
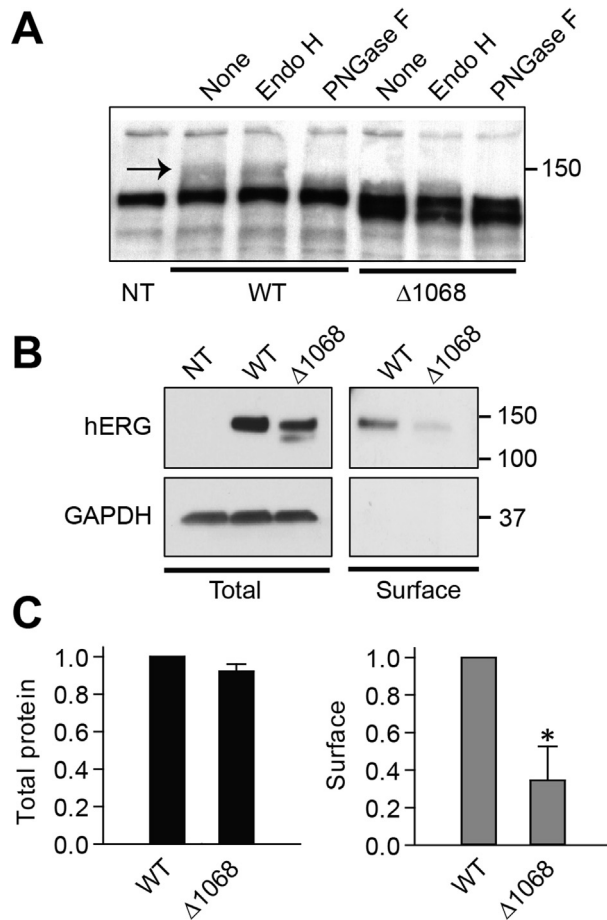
Fig. 3. Reduced surface expression of hERG-ΔQ1068 channels. (A) HEK-293 cells were transfected with 0.5 μg of wild-type hERG or hERG-ΔQ1068 cDNAs. Cell lysates were treated with Endo H, PNGase F or no treatment before subjecting to immunoblotting with an anti-hERG antibody. The 150 kDa band representing the mature, fully-glycosylated form is illustrated with an arrow. (B) HEK-293 cells were transfected with 2 μg of wild-type hERG or hERG-ΔQ1068 cDNAs. Live cells were surface biotinylated, cell lysates were prepared, and purified with streptavidin-agarose beads. The cell lysates, or biotinylated samples, were subjected to Western blotting with anti-hERG antibodies, or anti-GAPDH antibodies as a loading control. GAPDH was not observed in the surface biotinylated protein pool, verifying the identity of the sample. (C) Total hERG protein of wild-type hERG (n = 3) and hERG-ΔQ1068 (n = 3) in cell lysates was calculated by expressing the band intensities as a function of that of GAPDH. The two hERG-ΔQ1068 bands were summed to calculate expression of the variant. Surface expression was calculated by expressing their band intensities relative to total protein respectively for wild-type hERG (n = 3) or hERG-ΔQ1068 (n = 3). $p < 0.05$ with a Student's t-test.

better assess changes in surface expression, we performed surface biotinylation assays with HEK-293 cells transfected with 2 μg of the cDNAs, to increase the ratio of overexpressed/endogenous protein. Indeed, these experiments showed that the surface biotinylated hERG-ΔQ1068 protein was significantly less than wild-type hERG without alterations in total expression (Fig. 3B and C). This experiment demonstrates that ΔQ1068 hERG causes a trafficking defect, without affecting protein stability or degradation.

3.3.3. hERG-ΔQ1068 accelerates gating kinetics

We next studied the effects of ΔQ1068 on the time course of the activation process (opening of the activation gates) by using an "envelope of tails" method. The amplitude of the tail current during repolarization from a conditioning voltage at 20 mV (which gradually opens the activation gates) to -100 mV is directly proportional to the number of open activation gates at the end of the preceding depolarizing step. The time course of activation was determined by plotting the tail current amplitude as a function of the duration of preceding depolarization step (Fig. 4A and B). Subjecting these data points to curve fitting with a single exponential function shows that hERG-ΔQ1068 activated with a time constant of 82 ± 5.3 ms (n = 6), which was significantly more rapid than wild-type (144 ± 8.2 ms, n = 6, p < 0.05). Deactivation kinetics (re-closing of the activation gates upon repolarization) was obtained by curve fitting of the tail currents in Fig. 4C to a sum of two exponential functions. Deactivation was strongly voltage dependent, with the time constants of both the
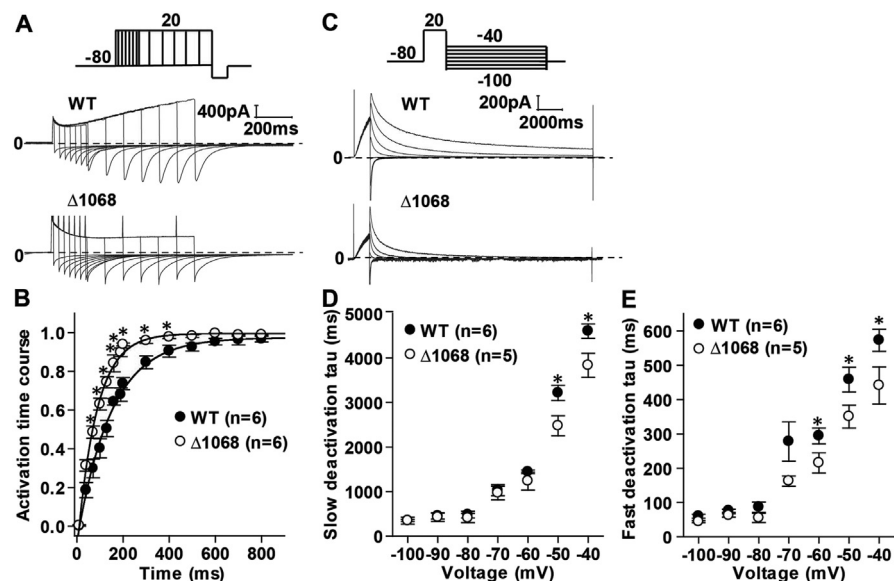
Fig. 4. Effects of hERG-ΔQ1068 on activation kinetics. (A) Representative trace demonstrating the measurement of the time course of activation. From the holding potential of -80 mV, the membrane was clamped to +20 mV for various durations before repolarizing to -100 mV for 2000 ms. (B) The tail current amplitudes at -100 mV were normalized to maximal tail current amplitude and plotted as a function of the preceding depolarization duration to produce the "envelope of tail currents". Data points were subjected to curve fitting to a single exponential function, normalized current = $1-e^{-t/\tau}$, where t is time and τ is the activation time constant. (C) Representative trace to demonstrate the recording of deactivation kinetics. From a holding potential of -80 mV, the membrane was clamped to 20 mV for 1000 ms, followed by repolarization for 14 ms to test voltages between -40 mV and -100 mV. Tail current data points were subjected to curve fitting to a two exponential function, $f(t) = [A_f * \exp (t_f/\tau_f)]+ [A_s * \exp (t_s/\tau_s)]+C$, with A the amplitude, τ the deactivation time constant and c the offset parameter. (D and E) Summary data respectively of the slow and fast deactivation time constants. Data points represent mean ± SEM. *p < 0.05 with Student's t-test.

fast (Fig. 4D) and slow (Fig. 4E) components of deactivation increasing with membrane depolarization. Both fast and slow components of deactivation occurred more rapidly for hERG-ΔQ1068 compared to wild-type (Fig. 4E and D).

### 3.3.4. Effects of ΔQ1068 on inactivation properties

We next performed experiments to determine whether the ΔQ1068 C-terminal truncation affects inactivation properties of the channel by examining the behavior of the inactivation gate at steady-state (Fig. 5A). hERG channels are unique in that inactivation occurs much more rapidly than activation. After clamping to a positive voltage (+20 mV) to open the activation gates, conditioning voltage clamp step of 20 ms was applied, during which deactivation is insignificant, but the inactivation gates open fully. Returning the membrane potential to 20 mV results in a tail current, with an amplitude a function of the fraction of inactivated states in the open state at the end of the preceding test voltage. The steady-state inactivation curve is produced by plotting the normalized tail currents as a function of the test potential (Fig. 5B). This analysis shows that voltage at which half-maximal steady-state inactivation occurs was shifted to positive voltages for hERG-ΔQ1068. By itself, this voltage shift represents a gain-of-function phenotype since more inactivation gates are open at steady-state at any given voltage.

3.3.5. Diminished cumulative activation of hERG-ΔQ1068

Some of the effects of hERG-ΔQ1068 are consistent with a loss-of-function phenotype, such as the reduced current density, reduced surface expression and accelerated deactivation. Other effects, however, are consistent with a gain-of-function phenotype, including the negative voltage shift of steady-state activation curve, the positive shift of the steady-state inactivation curve, and accelerated activation. To resolve these apparent contradictory phenotypes, we assessed cumulative activation using a rapid pacing protocol, which demonstrated that wild-type hERG progressively increases over time as more channels enter the activated state (Fig. 6). The hERG-ΔQ1068 channel, in contrast, completely lacked cumulative activation, demonstrating that a loss-of-function predominates, particularly at rapid heart rates.

3.3.6. WT failed to rescue hERG-ΔQ1068 in the heterozygous state

To simulate the heterozygous state in the decedent, experiments were performed with COS-7 cells co-transfected with wild-type and hERG-ΔQ1068 cDNAs. Transfection 1 μg WT hERG cDNA alone led to a current amplitude that was ~30 pA/pF at -40 mV, whereas transfection with 0.5 μg WT hERG cDNA led to a current that was ~50% smaller (not shown). As expected, the hERG-
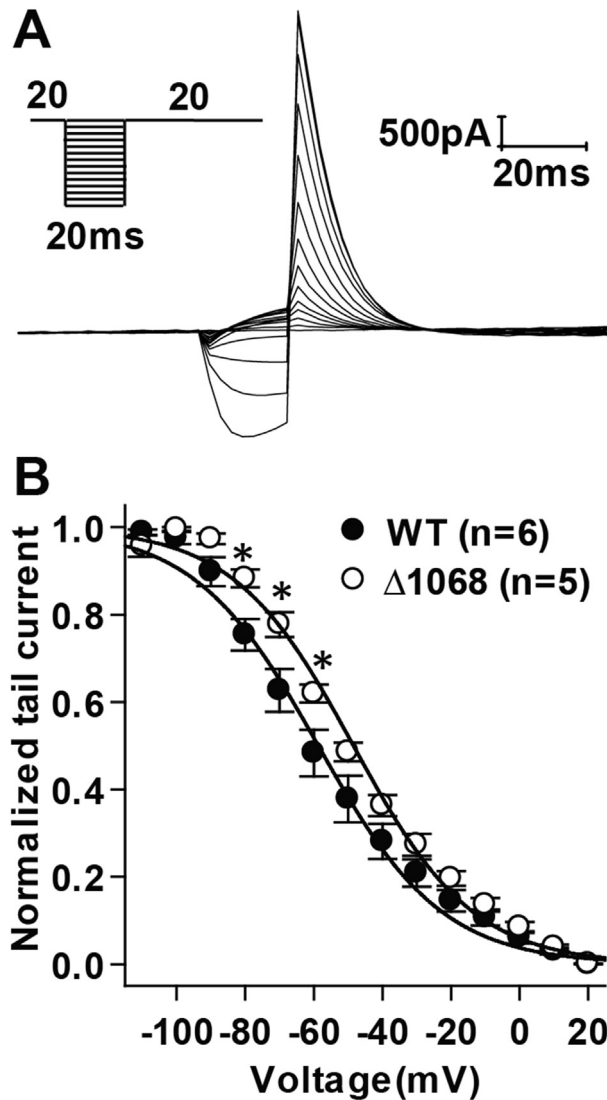
Fig. 5. Voltage dependence of steady-state inactivation. (A) A typical recording demonstrating the method. From a holding potential of -80 mV, the membrane was clamped to 20 mV for 500 ms, followed by a conditioning pulse of 20 ms between -110 and +20 mV, before measuring tail current amplitudes during a test pulse of 800 ms at 20 mV. The protocol was repeated every 15 s. (B) Tail current amplitudes were normalized to the maximal tail amplitude and plotted against the conditioning voltage to obtain the steady-state inactivation curve. Data points were subjected to curve fitting to a modified Boltzmann equation, $y = 1/[1+\exp[(V_m-V_{1/2})/k]]$, where $V_{1/2}$ is the voltage of half-maximal inactivation, and k represents the slope factor. Data points represent mean $\pm$ SEM. *$p < 0.05$ with Student's t-test.

ΔQ1068 current density was significantly smaller relative to wild-type (Fig. 7A, B and C). Co-transfecting cells with 0.5 μg each of wild-type WT and ΔQ1068 did not further reduce current amplitude This occurred in the absence of unexpected changes in protein levels (Fig. 7D). These data demonstrate haploinsufficiency of the heterozygous state.
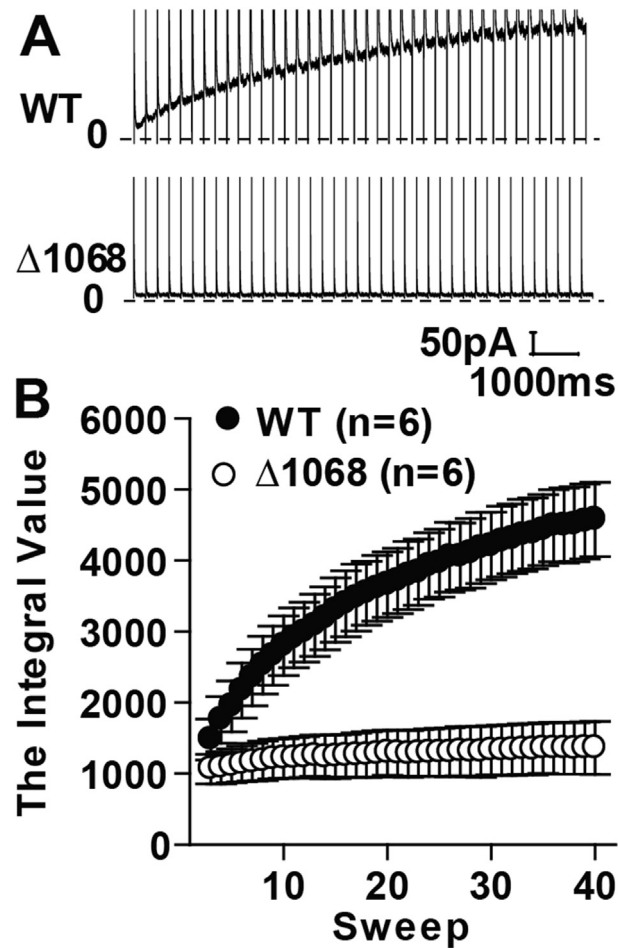
Fig. 6. hERG currents recorded using rapid repetitive pulses as the command waveform. (A) Slow time scale recording of wild-type hERG or hERG-ΔQ1068 during 250 ms voltage clamp steps from -88 mV to 0 mV, repeated at 4 Hz. (B) The total current during the depolarization step was integrated and corrected for cell size, and plotted as a function of the pulse number. Data points represent mean ± SEM. *p < 0.05 with Student's t-test.

3.4. Variant classification using 2015 ACMG-AMP guidelines

We classified the NP_000229.1:p.Gln1068Ter variant based on 2015 ACMG-AMP evidence-weighted sequence variant guidelines:

- PVS1 - Predicated null variant in a gene where loss-of-function is a known mechanism of disease. Haploinsufficiency score for *KCNH2* gene is 3 in ClinGen. (https://www.ncbi.nlm.nih.gov/projects/dbvar/clingen/clingen_gene.cgi?sym=*KCNH2*&subject). The p.Gln1068Ter variant is predicted to cause a replacement of the amino acid glutamine with a premature stop codon at position 1068 of the *KCNH2* gene encoded protein (total 1159 amino acids).

- PS3 - Well-established functional study showed a deleterious effect.
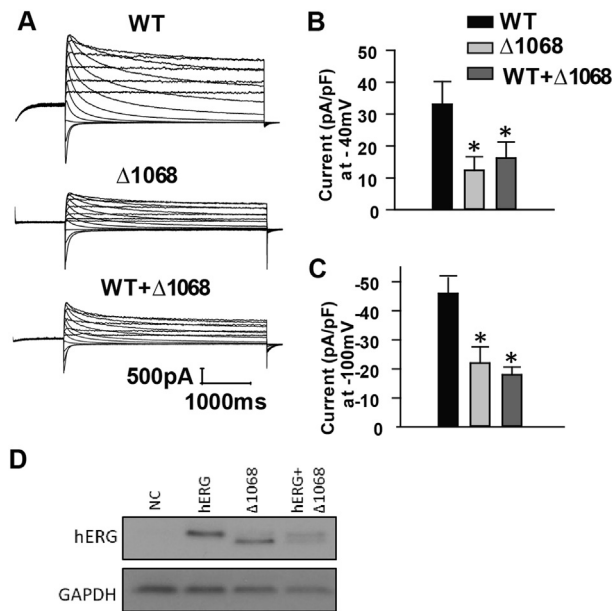
Fig. 7. Simulated heterozygosity of the ΔQ1068 variant. COS-7 cells were transfected with 1 μg wild-type hERG (WT), 1 μg hERG-ΔQ1068, or 0.5 μg each of wild-type or hERG-ΔQ1068 cDNAs and subjected to whole-cell patch clamping. (A) The fully-activated hERG currents were recorded as described in Fig. 2. Currents at -40 mV (B) or -100 mV (C) were corrected for cell surface area by dividing by the capacitance, averaged and displayed as bar graphs. (D) Western blotting with an anti-hERG antibody of cell lysates of the three experimental groups. The error bars represent SEM. *$p < 0.05$ with Student's t-test.

- PM2 - Absent in population databases: The p.Gln1068Ter variant is not found in the ESP6500 data from NHLBI Grand Opportunity Exome Sequencing Project (ESP), in the Exome Aggregation Consortium (ExAC), or in gnomAD.

- PM6 - This variant is a *de novo* (without paternity confirmation).

- PP4 - This variant is consistent with the decedent's ante-mortem history of prolonged QT interval on electrocardiogram.

In summary, evidence for classifying the NP_000229.1:p.Gln1068Ter variant include one very strong evidence (PVS1), one strong evidence (PS3), two moderate evidence (PM2 and PM6) and one supporting evidence (PP4); therefore, this variant is classified as pathogenic.

3.5. Effective precision healthcare for family members through molecular autopsy

From the perspectives of quality, cost and time effectiveness, we compared the healthcare for family members with (Fig. 8A) or without molecular autopsy (Fig. 8B) using a three-generation family model consisting of parents, five siblings
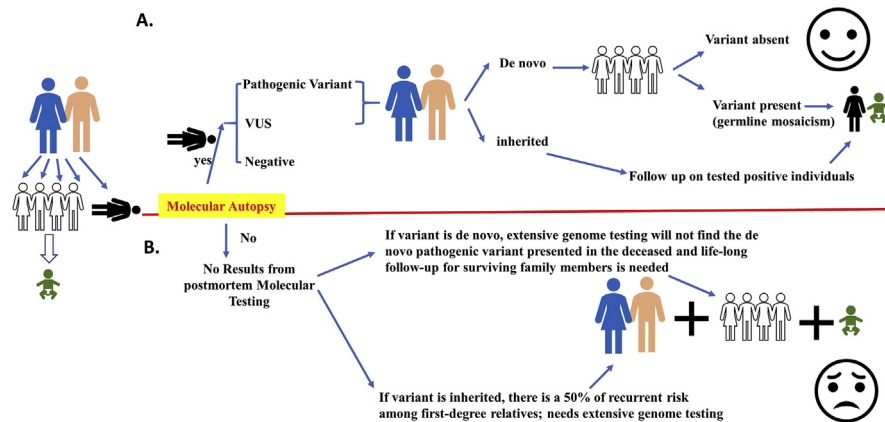
Fig. 8. Comparison of the Healthcare for Surviving Family Members. Cost, time and quality of healthcare for surviving family members with (A) or without molecular autopsy (B) using a three-generation family of parents, five siblings and a grandchild as an example where one of the siblings died suddenly and unexpectedly in an undetermined cause of natural death.

and a grandchild where one of the siblings died suddenly and unexpectedly of an undetermined natural cause.

- When molecular autopsy is performed (Fig. 8A), there are three possibilities of the testing results: the presence of pathogenic/likely pathogenic (P/LP) variants, VUS, or benign/likely benign (B/LB) variants (negative). Testing biological parents would determine whether a P/LP or VUS was *de novo* or inherited. When a P/LP variant is *de novo*, the siblings could be tested for the *de novo* variant due to the low possibility of germline mosaicism. Familial variant testing should be timed with clinical evaluation. If none carry the variant, there is no need for further testing. When a P/LP variant is inherited, then targeted clinical evaluation of the carriers and cascade testing of other at-risk family members, such as their children should be pursued. Non-carriers would not need further evaluation. Genotype-phenotype evaluation of the family members would also be valuable to understand a VUS found in the decedent. This approach leads to cost and time effective precision healthcare of the family members.

- When molecular autopsy is not performed (Fig. 8B), the presence of a P/LP or VUS, its status as *de novo* or inherited, or its relationship to the cause of death would be entirely unknown. The family would need to be evaluated and managed due to a positive family history of sudden death, which would entail life-long yearly screening in the form of EKGs and echocardiograms, as well as a diagnostic odyssey of exhaustive genetic testing for all family members. In the scenario where a P/LP variant is *de novo* and only present in the decedent, no genetic testing (not even whole genome testing) of the surviving family members would yield a meaningful result and they would have to be followed indefinitely. A possible alternative scenario is if a VUS is found in family members, tested in the absence of any phenotype and only because

of family history, it could be falsely attributed to the decedent's cause of death, leading to unnecessary and potentially dangerous treatment in family members, based on the incorrect interpretation of the VUS as the probable substrate for the relative's death. Conversely, if the variant linked to the sudden death in the index case is unknown for lack of molecular autopsy, but present in other surviving family members, there could be either a risk of a recurrent death, or unnecessary care for all the surviving family members, including unaffected, both costly and time-consuming for the patients and the healthcare system.

The cost varies by commercial laboratories, geographic locations, as well as types of clinical practice. Here we focused on the *relative cost-saving* in healthcare of surviving family members with and without molecular autopsy. When molecular autopsy is performed, the healthcare cost involves targeted variant testing for the survival family members (approximately $400 per person) and clinical evaluation (approximately $300 for visit with EKG ($50) and Echo ($1500) per person) [13, 14]. If there is a *de novo* pathogenic variant, the total cost of care is approximately $2300 per person (around $14,000 total for the parents and four siblings); if one of the family members inherits a pathogenic variant found through molecular autopsy, yearly clinical evaluation of the affected individual with standard care cost follows. On the other hand, when molecular autopsy is not performed, coats rise to approximately $5,000 for a clinical whole-exome study per person [15], and yearly clinical evaluation ($300) with EKG ($50) and Echo ($1500) per person and any future children for the remainder of their lives [13, 14]. The total cost of care could easily get into hundreds of thousands of US dollars for the family over time.

4. Discussion

This study has two important messages: 1) molecular autopsy enabled an accurate determination of the cause of death for the 18-year-old woman who died suddenly and unexpectedly; and 2) molecular autopsy enabled cost-effective and quality healthcare for the surviving first-degree family members (a total of six people in this case). As no one carried the *de novo* pathogenic variant, there is no risk for recurrent sudden death from the same condition, no need for additional extensive genome testing or yearly follow-up for any of them, and more importantly, no chance of being over treated due to a suspicious VUS. This result will also impact future generations.

De novo variants are increasingly recognized as important causes of health conditions as the field of human genetics shifts from positional mapping of disease loci in large pedigrees with multiple affected members to NGS testing of affected and

parents (trio-based) [16]. As such, *de novo* variants are now well appreciated in severe early-onset disease, even though it is less documented in late-onset diseases, largely due to lack of parental samples for older patients. Recent clinical exome sequencing studies have shown that 60−75% of all sporadic cases that received a molecular diagnosis could be explained by *de novo* mutations [17, 18]. The majority of pathogenic *de novo* mutations manifest in a dominant manner. *De novo* variants have also been reported in diseases underlying the cause of sudden expected natural deaths, such as cardiac channelopathy [19], cardiomyopathy [20], epilepsy [21], etc. For example, *de novo* variants can explain up to 20% of cases of non-familial Brugada syndrome [22]. In a published cohort of 28 sudden death in the young (SDY) [23], about 50% of pathogenic variants resulted from *de novo* alterations. Besides *de novo* variants, the identification of an inherited variant would also enable targeted cascade variant testing in family members and genotype-phenotype correlation through clinical evaluations as we have previously reported [1, 2, 3].

Our electrophysiological characterization of the *KCNH2* variant introduced into transfected cells found that it resulted in loss-of function (reduced current density, reduced surface expression and accelerated deactivation) hallmarks, which can't be rescued by wild type, a finding consistent with a haploinsufficiency phenotype in the heterozygous state as previously shown in *in silico* models of cardiac electrophysiology [24]; the results are also consistent with functional studies for two nonsense *KCNH2* variants, p.Q725TER and p.R1014TER [25], both are upstream of our variant (p.Gln1068Ter). As the identified premature stop codon occurs more than 50 bp upstream of the normal stop codon, it is also possible that there exists the nonsense mediated decay mechanism that we are not tested in this study. A RNAseq analysis of affected heart tissue would be considered for a future study.

Among the loss-of-function variants close to our variant in *KCNH2* which have been reported previously, one is the p.Gln1068Thrfs, which was reported as a pathogenic variant in ClinVar without phenotype information [26]; another is the p.Gln1070Ter which led to miscarriage and intrauterine fetal loss in the homozygous states, although the heterozygote parents only showed borderline long QT [27]. We noticed the decedent in our study had marked QTc prolongation as a heterozygote, for which there may be additional genetic or environmental modifiers at play that are not discovered in this study. Therefore, it would be prudent for the family members to avoid agents (e.g. medications) known to prolong QTc. Among family members, we did not appreciate a difference in QT duration that could distinguish carriers of the *CACNA1D* variant from non-carriers, so the role of that specific "hit" in influencing QT duration is unlikely or minimal. In addition, other studies have shown nonsense variants leading to a similar QTc interval as we observed, or even a more severe phenotype at younger ages [28, 29], although the correlation of a specific genotype to a phenotype lacked in cohort-based studies.

Applying molecular autopsy to death investigation has yielded impactful results to families all over the world [5, 23, 30, 31]. Over the past 15 years, our office has become the first and only medical examiner's office in the United States to *routinely* perform molecular autopsy in sudden unexpected deaths in-house. The forward-thinking leadership in New York City decided to utilize existing resources (lab space, instruments, personnel, etc.) through the largest forensic laboratory in the nation, to build an in-house College of American Pathologists (CAP)-accredited molecular genetics laboratory, and to provide on-site family counseling through board-certified genetic counselor. The National Institute of Justice has also substantially supported the technology expansion to massive parallel sequencing, functional study and genetic counseling through several research grants. We have published our work on testing for thrombophilia [6, 32] and for cardiac arrhythmogenic genes [1, 3, 4, 5], and we expect to add testing for other inheritable conditions at risks for sudden death, such as epilepsy and aortopathy soon. Joining other studies that described recommendations for molecular autopsy [31, 33], we have outlined an example of best practice of postmortem diagnosis and effective care for the survival family members in this manuscript. However, molecular autopsy is not routinely being used in sudden unexpected natural deaths investigations in other parts of the United States, primarily due to lack of sustainable funding support and medical coverage, leaving thousands of cases untested and poor clinical care for at-risk family members [23].

5. Conclusion

We demonstrated effective precision healthcare of surviving family members (six in this case) through in-depth study of a novel *de novo* pathogenic variant in the Long QT syndrome type 2 gene *KCNH2*. As molecular autopsy saves money, time and efforts, and removes psychological stress and anxiety from the healthcare of surviving family members, we advocate a reform of the U.S. healthcare system by including molecular autopsy through the care of the first-degree relatives. "*Hic locus est ubi mors gaudet succurrere vitae* — this is the place where the dead are pleased to help the living"; we feel strongly that it is our professional duty to advocate for the healthcare coverage of molecular autopsy for the betterment of humanity.

Declarations

Author contribution statement

Yingying Tang: Conceived and designed the experiments; Analyzed and interpreted the data; Contributed reagents, materials, analysis tools or data; Wrote the paper.

Jingyun Dong: Conceived and designed the experiments; Performed the experiments; Analyzed and interpreted the data.

William Coetzee: Conceived and designed the experiments; Analyzed and interpreted the data.

Nori Williams: Performed the experiments; Analyzed and interpreted the data.

Marina Cerrone, Christopher Borck, Dawei Wang, Bo Zhou, Lucy Eng, Sung Yon Um, Ying Lin, Kevin Ruiter, Lisa Rojas: Performed the experiments.

Barbara Sampson: Conceived and designed the experiments.

Funding statement

Competing interest statement

The authors declare no conflict of interest.

Additional information

No additional information is available for this paper.

References

[1] I. Gando, J. Morganstein, K. Jana, T.V. McDonald, Y. Tang, W.A. Coetzee, Infant sudden death: mutations responsible for impaired Nav1.5 channel trafficking and function, Pacing Clin. Electrophysiol. 40 (2017) 703−712.

[2] J. Chen, M. Weber, S.Y. Um, C.A. Walsh, Y. Tang, T.V. McDonald, A dual mechanism for I(Ks) current reduction by the pathogenic mutation KCNQ1-S277L, Pacing Clin. Electrophysiol. 34 (2011) 1652−1664.

[3] Y. Krishnan, R. Zheng, C. Walsh, Y. Tang, T.V. McDonald, Partially dominant mutant channel defect corresponding with intermediate LQT2 phenotype, Pacing Clin. Electrophysiol. 35 (2012) 3−16.

[4] B.A. Sampson, Y. Tang, Holistic approach to determine cause of autopsy-negative sudden natural death, J. Am. Coll. Cardiol. 69 (2017) 2146−2148.

[5] Y. Lin, N. Williams, D. Wang, et al., Applying high-resolution variant classification to cardiac arrhythmogenic gene testing in a demographically diverse cohort of sudden unexplained deaths, Circ. Cardiovasc. Genet. 10 (2017).

[6] M. Halvorsen, Y. Lin, B.A. Sampson, et al., Whole exome sequencing reveals severe thrombophilia in acute unprovoked idiopathic fatal pulmonary embolism, EBioMedicine 17 (2017) 95−100.

[7] Considerations in healthcare reform for patients and families with genetic diseases: a statement of the American College of Medical Genetics and Genomics, Genet. Med. 20 (2018) 561.

[8] N. Williams, R. Marion, T.V. McDonald, et al., Phenotypic variations in carriers of predicted protein-truncating genetic variants in MYBPC3: an autopsy-based case series, Cardiovasc. Pathol. 37 (2018) 30−33.

[9] J.T. den Dunnen, R. Dalgleish, D.R. Maglott, et al., HGVS recommendations for the description of sequence variants: 2016 update, Hum. Mutat. 37 (2016) 564−569.

[10] S. Richards, N. Aziz, S. Bale, et al., Standards and guidelines for the interpretation of sequence variants: a joint consensus recommendation of the American College of medical genetics and genomics and the association for molecular pathology, Genet. Med. 17 (2015) 405−424.

[11] C.T. Rueden, J. Schindelin, M.C. Hiner, et al., ImageJ2: ImageJ for the next generation of scientific image data, BMC Bioinf. 18 (2017) 529.

[12] R.W. Sy, C. van der Werf, I.S. Chattha, et al., Derivation and validation of a simple exercise-based algorithm for prediction of genetic testing in relatives of LQTS probands, Circulation 124 (2011) 2187−2194.

[13] E.J. Emanuel, A. Glickman, D. Johnson, Measuring the burden of health care costs on US families: the affordability index, J. Am. Med. Assoc. 318 (2017) 1863−1864.

[14] M.J. O'Grady, G.S. Wunderlich (Eds.), Medical Care Economic Risk: Measuring Financial Vulnerability from Spending on Medical Care, 2013. Washington (DC).

[15] K. Schwarze, J. Buchanan, J.C. Taylor, S. Wordsworth, Are whole-exome and whole-genome sequencing approaches cost-effective? A systematic review of the literature, Genet. Med. (2018).

[16] R. Acuna-Hidalgo, J.A. Veltman, A. Hoischen, New insights into the generation and role of de novo mutations in health and disease, Genome Biol. 17 (2016) 241.

[17] Y. Yang, D.M. Muzny, F. Xia, et al., Molecular findings among patients referred for clinical whole-exome sequencing, J. Am. Med. Assoc. 312 (2014) 1870−1879.

[18] J.E. Posey, J.A. Rosenfeld, R.A. James, et al., Molecular diagnostic experience of whole-exome sequencing in adult patients, Genet. Med. 18 (2016) 678–685.

[19] C. Yin, P. Zhang, J. Yang, L. Zhang, Unique ECG presentations and clinical management of a symptomatic LQT2 female carrying a novel de novo KCNH2 mutation, J. Electrocardiol. 51 (2018) 111–116.

[20] A. Kiselev, R. Vaz, A. Knyazeva, et al., De novo mutations in FLNC leading to early-onset restrictive cardiomyopathy and congenital myopathy, Hum. Mutat. (2018).

[21] H. Saitsu, T. Akita, J. Tohyama, et al., De novo KCNB1 mutations in infantile epilepsy inhibit repetitive neuronal firing, Sci. Rep. 5 (2015) 15199.

[22] J.M. Juang, T.P. Lu, L.C. Lai, et al., Disease-targeted sequencing of ion channel genes identifies de novo mutations in patients with non-familial Brugada syndrome, Sci. Rep. 4 (2014) 6733.

[23] G.W. Shanks, D.J. Tester, S. Nishtala, J.M. Evans, M.J. Ackerman, Genomic triangulation and coverage analysis in whole-exome sequencing-based molecular autopsies, Circ. Cardiovasc. Genet. 10 (2017).

[24] S.A. Mann, M. Imtiaz, A. Winbo, et al., Convergence of models of human ventricular myocyte electrophysiology after global optimization to recapitulate clinical long QT phenotypes, J. Mol. Cell. Cardiol. 100 (2016) 25–34.

[25] Q. Gong, D.R. Keeney, J.C. Robinson, Z. Zhou, Defective assembly and trafficking of mutant HERG channels with C-terminal truncations in long QT syndrome, J. Mol. Cell. Cardiol. 37 (2004) 1225–1233.

[26] M.J. Landrum, J.M. Lee, M. Benson, et al., ClinVar: public archive of interpretations of clinically relevant variants, Nucleic Acids Res. 44 (2016) D862–D868.

[27] Z.A. Bhuiyan, S. Al-Shahrani, A.S. Al-Khadra, et al., Clinical and genetic analysis of long QT syndrome in children from six families in Saudi Arabia: are they different? Pediatr. Cardiol. 30 (2009) 490–501.

[28] C. Burns, J. Ingles, A.M. Davis, et al., Clinical and genetic features of Australian families with long QT syndrome: a registry-based study, J. Arrhythm. 32 (2016) 456–461.

[29] D.J. Tester, M.L. Will, C.M. Haglund, M.J. Ackerman, Compendium of cardiac channel mutations in 541 consecutive unrelated patients referred for long QT syndrome genetic testing, Heart Rhythm 2 (2005) 507–517.

[30] L. Marcondes, J. Crawford, N. Earle, et al., Long QT molecular autopsy in sudden unexplained death in the young (1-40 years old): lessons learnt from an eight year experience in New Zealand, PLoS One 13 (2018), e0196078.

[31] N. Lahrouchi, H. Raju, E.M. Lodder, et al., Utility of post-mortem genetic testing in cases of sudden arrhythmic death syndrome, J. Am. Coll. Cardiol. 69 (2017) 2134−2145.

[32] Y. Tang, B. Sampson, S. Pack, et al., Ethnic differences in out-of-hospital fatal pulmonary embolism, Circulation 123 (2011) 2219−2225.

[33] R.D. Bagnall, R.G. Weintraub, J. Ingles, et al., A prospective study of sudden cardiac death among children and young adults, N. Engl. J. Med. 374 (2016) 2441−2452.